Perylene Diimide-Based Low-Cost and Thickness-Tolerant Electron Transport Layer Enables Polymer Solar Cells Approaching 19% Efficiency

ADVANCED FUNCTIONAL MATERIALS
www.afm-journal.de

Perylene Diimide-Based Low-Cost and Thickness-Tolerant Electron Transport Layer Enables Polymer Solar Cells Approaching 19% Efficiency

Bin Zhang, Yushou Zhao, Congdi Xu, Chuang Feng, Wenming Li, Xiaofeng Qin, Menglan Lv,* Xuanyan Luo, Xiaolan Qin, Aiqing Li, Zhicai He,* and Ergang Wang**

The materials for electron transport layers (ETLs) play a significant role in the performance of polymer solar cells (PSCs) but face challenges, such as low electron transport mobility and conductivity, low solution processibility, and extreme thickness sensitivity, which will undermine the photovoltaic performance and hinder compatibility of large-scale fabrication technique. To address these challenges, a new n-type perylene diimide-based molecule (PDINB) with two special amine-anchored long-side chains is designed and synthesized feasibly. PDINB shows very high solubility in common organic solvents, such as dichloromethane (>75 mg ml^{-1}) and methanol with acetic acid as an additive (>37 mg ml^{-1}), which leads to excellent film formability when deposited on active layers. With PDINB as ETLs, the photovoltaic performance of the PSCs is boosted comprehensively, leading to power conversion efficiency (PCE) up to 18.81%. Thanks to the strong self-doping effect and high conductivity of PDINB, it displays an appreciable thickness-tolerant property as ETLs, where the devices remain consistently high PCE values with the thickness varying from 5 to 30 nm. Interestingly, PDINB can be used as a generic ETL in different types of PSCs including non-fullerene PSCs and all-polymer PSCs. Therefore, PDINB can be a potentially competitive candidate as an efficient ETL for PSCs.

1. Introduction

Silicon and copper indium gallium selenide (CIGS) solar cells have demonstrated successful conversion of solar energy to electricity. Nevertheless, their progress is impeded by challenges such as high production costs, substantial weight, and emerging recycling concerns, which constrain their further development. Polymer solar cells (PSCs), on the other hand, have obtained much attention ascribing to their novel merits in light weight, low cost, flexibility, large-scale fabrication, and so on.[1] Under the persistent efforts of researchers, the power conversion efficiency (PCE) has exceeded 19% in the single-junction PSCs,[2,3] which demonstrates that PSCs are potentially competitive as candidate for solar energy conversion in the future.

It is known that PSCs are composed of three important layers, namely, the hole transport layer (HTL), active layer, and electron transport layer (ETL) sandwiched between two electrodes. Many HTL materials have been developed, with PEDOT:PSS and its derivatives standing out as extensively utilized HTL in PSCs, attributing to its advantages of suitable work function, high hole conductivity, and excellent film-forming ability.[4,5] At the same time, significant advancements have been made in the development of the active layer, comprising both electron-donating and electron-accepting materials, over the past decades. One of the remarkable developments

B. Zhang, Y. Zhao, W. Li, X. Qin, M. Lv, X. Luo, X. Qin, A. Li
Engineering Research Center for Energy Conversion and Storage Technology of Guizhou
School of Chemistry and Chemical Engineering
Guizhou University
Guiyang 550025, China
E-mail: zhangb@gzu.edu.cn; mllv@gzu.edu.cn

C. Xu, C. Feng, Z. He
Institute of Polymer Optoelectronic Materials and Devices
State Key Laboratory of Luminescent Materials and Devices
South China University of Technology
Guangzhou 510640, China
E-mail: zhicaihe@scut.edu.cn

E. Wang
Department of Chemistry and Chemical Engineering
Chalmers University of Technology
Göteborg SE-412 96, Sweden
E-mail: ergang@chalmers.se

The ORCID identification number(s) for the author(s) of this article can be found under https://doi.org/10.1002/adfm.202400903

DOI: 10.1002/adfm.202400903

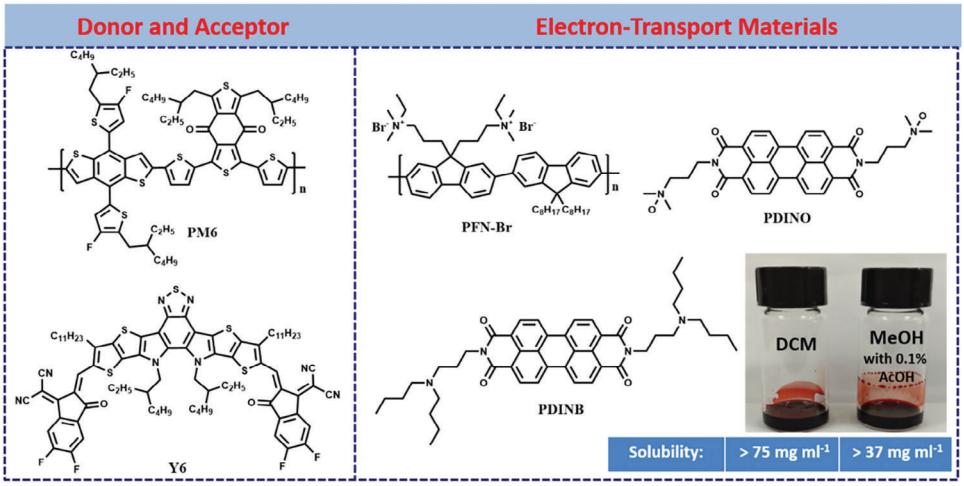

Figure 1. The chemical structures of the donor, acceptor materials, and ETLs.

can be attributed to the emergence of A-D-A (acceptor-donor-acceptor) type non-fullerene electron-accepting molecules.[6–8] Throughout this period, numerous outstanding donors and acceptors have been efficiently created, including donor polymers like PM6,[9] D18,[10] and PTQ10,[11] and electron acceptors such as ITIC,[12] Y6,[7] and PY-IT.[13] On the other hand, the electron-transport materials, as another indispensable layer in PSCs, have been playing a very important role in enhancing the photovoltaic performance. In the past, many types of ETLs have been discovered and developed, including inorganic materials, conjugated and non-conjugated small molecular electrolytes, conjugated and non-conjugated polyelectrolytes, nano-carbon-based materials, and metal oxides.[14–18] Compared with the inorganics and metal oxides, the organics and polymers are regarded as a promising alternative as ETLs such as PFN,[19] PFN-Br,[20] PDIN,[21] PDINO,[21] PDINN,[22,23] and PNDIT-F3N,[24] resulting from their merits in low cost, feasible functionalization, excellent solution-processability, and easy tuning of energy levels. Despite of the development of ETLs, challenges persist, including issues like poor thickness-tolerance and high production cost. Hence, there is an urgent need to design and develop an efficient ETL to advance PSCs.

There are prerequisites for efficient ETLs, including high electron mobility, high conductivity, a reduction of the work function of the cathode, excellent solution processibility, good stability, and cost-effectiveness. Among these ETLs, the perylene diimide (PDI) based materials, such as, PDIN, PDINO, and PDINN, exhibit promising properties as efficient ETLs in PSCs.[21,23] Taking advantages of PDI-based ETLs, a modified PDIN derivative (PDIN-TEMPO) was created via introducing a stable radical unit of TEMPO to PDIN backbone. Ascribing to the electron-conducting nature of TEMPO, the PDIN-TEMPO showed high photovoltaic performance in PSCs, indicating that the introduction of stable radicals to PDI-based derivatives would be an efficient strategy for developing novel ETLs.[25] However, these PDI derivatives also suffer from the abovementioned challenges. To address these challenges, a novel PDI derivative of 2,9-bis(3-(dibutylamino)propyl)perylene diimide (PDINB) was synthesized via introducing branched long side chains to the PDI core. Through the new design, the PDINB shows very high solubilities in common organic solvents such as dichloromethane (DCM) (>75 mg ml^{-1}) and methanol (MeOH) with 0.1 (v/v)% acetic acid (AcOH) (> 37 mg ml^{-1}), which are among the highest solubilities for PDI-based ETLs. This high solubility in MeOH can ensure excellent film-forming property when depositing PDINB on the active layers. Furthermore, the introduction of long side chains in PDI increases the flexibility of amine chains, leading to elevated capability of self-doping effect. Ultimately, PDINB features high conductivity and excellent ohmic contact in PSCs, where it presents the thickness-insensitive property as ETL in PSCs. Interestingly, it shows broad applicability as ETLs in different types of PSCs devices, including small molecular acceptor-based devices and all-polymer PSCs. Hence, PDINB exhibits very promising properties as efficient ETLs, which will possibly be compatible with large-area roll-to-roll processing for PSCs.

2. Results and Discussion

2.1. Synthesis and Characterization

The synthetic route of PDINB was presented in Scheme S1 (Supporting Information). The synthesis of PDINB is very simply via a one-step general condensation reaction using commercially available 3,4,9,10-perylenetetracarboxylic dianhydride and *N,N*-dibutyl-1,3-propanediamine without any catalyst. The reaction yield is nearly quantitative (Scheme S1, Supporting Information). Interestingly, the product of PDINB does not require any additional purification processes as discussed in Supporting Information, which further simplified the synthesis of PDINB. Following the cost calculation, the cost of PDINB is ≈ $0.19 per gram (Table S1, Supporting Information). The cost of PDINB is much less than other commercial ETLs, indicating its potential for mass production. The chemical structure of PDINB is verified by both ^{1}H-NMR and ^{13}C-NMR as shown in Figures S1 and S2 (Supporting Information). It is widely noted that most of n-type interfacial materials present very low solubility. Here, we tested the solubility of PDINB in both nonpolar and polar solvents including DCM and MeOH. Surprisingly, PDINB shows very high

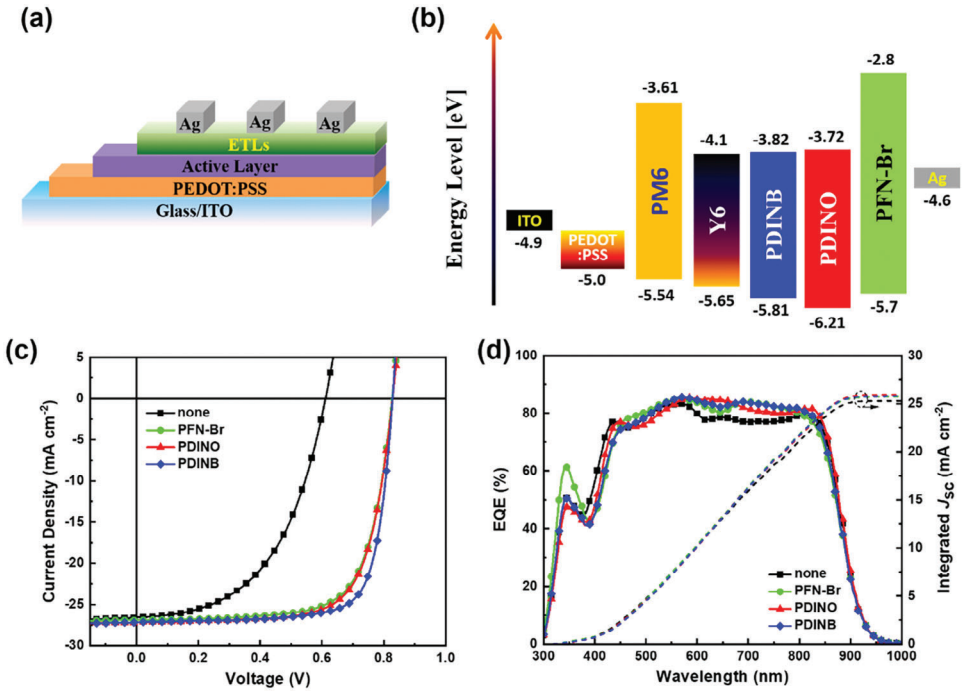

Figure 2. Device characterizations: a) device structure, b) energy level diagram, c) *J*--*V* curves, and d) EQE curves of the PSCs based on different ETLs.

solubility of >75 mg ml^{-1} in DCM and >37 mg ml^{-1} in MeOH with 0.1 (v/v) % AcOH (**Figure 1**), which is higher than other reported neutral ETLs (Table S2, Supporting Information). This high solubility is ascribed to the existence of four branched side chains, which is very beneficial for solution processibility when preparing uniform ETLs in PSCs. Thermogravimetric analysis (TGA) was employed to examine the thermal properties of PDINB, as shown in Figure S3 (Supporting Information). It presents a 5% weight loss occurring at ≈ 270 °C, suggesting that PDINB exhibits high thermal stability. To gain energy levels of PDINB, the electrochemical test was carried out to determine the highest occupied molecular orbital (HOMO) and lowest unoccupied molecular orbital (LUMO) levels, as shown in Figure S4 (Supporting Information). The HOMO and LUMO levels of PDINB are −5.81 and −3.82 eV, respectively, indicating that PDINB exhibits typical n-type characteristics for efficiently transporting electrons and blocking holes.

2.2. Photovoltaic Properties

To investigate the photovoltaic performance of PDINB as ETL in PSCs, the photovoltaic devices were prepared by using a conventional device architecture of glass/indium tin oxide (ITO)/poly(3,4-ethylenedioxythiophene):poly(styrenesulfonate) (PEDOT:PSS)/active layer/ETLs/Ag (**Figure 2a**); and the related energy level diagram was presented in Figure 2b. Here, we utilized the state-of-the-art PM6 and Y6 as the electron-donating polymer and electron-accepting small molecule in active layer, respectively. To compare with PDINB, the other two well-known ETL materials of PFN-Br and PDINO were also employed as ETLs in PSCs (Figure 1).

As shown in Figure 2c,d, the current density-voltage (*J*–*V*) and external quantum efficiency (EQE) curves of the PSCs based on PFN-Br, PDINO, and PDINB as ETLs are presented, respectively; and the related photovoltaic data are summarized in **Table 1**. All the devices with the three materials as ETLs exhibit much higher photovoltaic performance than the ones without ETL, which originate from the simultaneously improved open-circuit voltages (V_{OC}s), short-circuit currents (J_{sc}s), and fill factors (FFs). All the devices by using PFN-Br, PDINO, and PDINB as ETLs give high PCEs of over 15%, which are consistent with the previous reports on PSCs based on PFN-Br and PDINO.[22,26] Interestingly, the device with PDINB as ELT shows the highest photovoltaic performance among the PSCs based on different ETLs with V_{OC} of 0.83 V, J_{sc} of 27.08 mA cm^{-2}, FF of 76.85% and PCE of 17.34%. It is noticed that the improved performance for the PDINB-based device is mainly attributed to its higher FF as the J_{sc} and V_{OC} values are comparable. The higher FF value implies that PDINB as ETLs may behave more effective with interfacial modification and higher electron-transport properties, which is worthy of further investigation in the next sections. Moreover, the device stability is a very important characteristic for PSCs. Here, long-time stabilities of devices with different ETLs are also evaluated in N_2 without encapsulation. As shown in Figure S5 (Supporting Information), it is noted that the device without any ETLs presents a rapid roll-off, whereas the devices with ETLs demonstrate a slow roll-off. This result implies that the introduction of ETLs could effectively improve the device's stability. Furthermore, the device with PDINB presents the highest stability among those without an ETL and with PFN-Br and PDINO as ETLs, maintaining 80% of its initial PCE after 600 h. Therefore, PDINB emerges as a promising candidate, serving as an advantageous ETL capable of improving

Table 1. Summary of photovoltaic performance of the PSCs based on different ETLs under AM 1.5 G illustration.

ETLs	Thickness [nm]	V_{OC} [V]	J_{SC} [mA cm^{-2}]	$J^{b)}{}_{SC}$ [mA cm^{-2}]	FF [%]	PCE$_{avg}$ [a)] [%]	PCE$_{max}$ [%]
none	0	0.61	26.55	25.28	51.61	8.25 (±0.23)	8.40
PFN-Br	5	0.83	26.88	25.74	71.43	15.74 (±0.20)	15.93
PDINO	10	0.83	27.09	25.93	71.93	16.02 (±0.15)	16.18
PDINB	10	0.83	27.08	25.78	76.85	17.11 (±0.12)	17.34

[a)] the average PCE values from 10 individual devices; [b)] integrated J_{SC} from EQE curves.

photovoltaic performance and extending long-time stability of the device.

In the context of large-area, high-speed roll-to-roll processing, achieving precise control over the thickness of ETLs can be challenging. Consequently, there is a significant appreciation for photovoltaic performance that remains insensitive to variations in the thickness of ETLs. Herein, we evaluated the photovoltaic performance of PSCs with different thickness of PDINB as ETLs. As shown in **Figure 3** and **Table 2**, the PCEs exhibit an improvement from 16.56% to 17.34% as the thickness of PDINB increases from 5 to 10 nm. A slight decrease in device performance is observed when the thickness of PDINB is further increased to 20 and 30 nm, resulting in PCEs of 17.08% and 16.24%, respectively. Remarkably, even at the thickness of 40 nm, the photovoltaic performance remains at a high level with a V_{OC} of 0.83 V, J_{SC} of 25.7 mA cm^{-2}, FF of 71.04%, and PCE of 15.25%. It is noted that there is a subtle decrease in J_{sc} when the PDINB thickness increased to 40 nm, possibly ascribing to the increased interfacial resistance, which is consistent with the results from EQE (Figure 3b).[27] To further understand the effect of PDINB thickness on the device performance, the electron mobilities with different thickness of PDINB were tested via electron-only devices under the device architecture of ITO/ZnO/PM6:Y6/PDINB/Ag, where the electron mobilities were 9.43×10^{-4}, 2.06×10^{-3}, 1.35×10^{-3}, 1.26×10^{-3}, and 1.21×10^{-3} cm^2 V^{-1} s^{-1} for the PDINB thicknesses of 5, 10, 20, 30, and 40 nm, respectively (Figure S6, Supporting Information). Notably, the introduction of PDINB could improve the device electron mobility distinctly with a slight decrease when the thickness of PDINB is increased, indicating that efficient charge transport could be guaranteed even in the thick PDINB layer.[25] This thickness-tolerant capability of PDINB is higher than that of the devices with PFN-Br and PDINO as ETLs, as presented in Figure S7 and Table S3 (Supporting Information). Consequently, the photovoltaic performance of PSCs employing PDINB as ETLs demonstrates notable tolerance to variations in ETL thickness. This observation suggests that PDINB holds promise for applications in high-speed roll-to-roll processing.[28–30]

2.3. Interfacial Morphology Investigation

To further understand the reasons for different photovoltaic performances of the ETLs in PSCs, atomic force microscopy (AFM) images with the contact mode of the ETLs deposited on the PM6:Y6-based active layer were recorded. As presented in **Figure 4a–d**, the root-mean-square (rms) roughness of bare, PFN-Br, PDINO, and PDINB-modified active layer films from the AFM images are 4.32, 2.4, 4.68, and 4.92 nm, respectively. Although the PFN-Br-based film exhibits the lowest RMS roughness value, there are numerous protruding points, reaching as high as 6 nm dispersed across the active layer, which pose a disadvantage for the interfacial contact between the active layer and Ag cathode. Conversely, the surfaces deposited by PDINO and PDINB display a considerably more uniform coverage on the PM6:Y6 layer, potentially enhancing the interfacial contact and preventing direct contact between the active layer and Ag cathode. Interestingly, the PDINO-modified film reveals obvious crystalline nanofibril structures, likely attributing to its short side chains. In contrast, PDINB exhibits a more uniform morphology resulting from its reduced crystallinity due to its branched long side chains, which favors the desirable film-formability characteristics. Furthermore, to comprehend the wetting properties of the PM6:Y6 layers deposited by different ETLs toward Ag cathode, a detailed water contact angle test was performed, as shown in

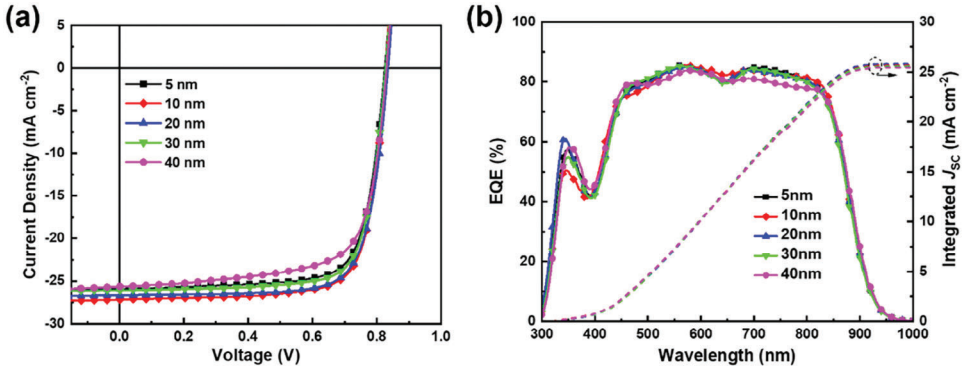

Figure 3. The *J*--*V* and EQE curves of PSCs based on PDINB as ETLs with different thicknesses under the device structure of ITO/ PEDOT:PSS/PM6:Y6/PDINB/Ag.

Table 2. Summary of photovoltaic properties of PSCs based on PDINB as ETLs with different thicknesses under AM 1.5 G illustration.

PDINB thickness (nm)	V_{OC} [V]	J_{SC} [mA cm^{-2}]	$J^{b)}_{SC}$ [mA cm^{-2}]	FF [%]	PCE$_{avg}$ [a)] [%]	PCE$_{max}$ [%]
5	0.83	26.24	25.69	75.95	16.35 (±0.08)	16.56
10	0.83	27.08	25.78	76.85	17.11 (±0.12)	17.34
20	0.84	26.69	25.64	76.32	16.70 (±0.31)	17.08
30	0.83	26.02	25.53	75.36	16.07 (±0.17)	16.24
40	0.83	25.70	25.45	71.04	15.12 (±0.13)	15.25

[a)] the average PCE values from 10 individual devices; [b)] integrated J_{SC} from EQE curves.

Figure 4e–h. The water contact angles are 100°, 71°, 40°, and 61° for bare, PFN-Br, PDINO, and PDINB-modified active layers, respectively. The results indicate that the pristine PM6:Y6 layer is inherently hydrophobic, while the PDINO-based film is quite hydrophilic. In comparison, the PFN-Br and PDINB-based films present intermediate polarity, which is conducive for forming improved contacts between the ETLs and Ag cathode. Comprehensively, PDINB exhibits superior interfacial contact properties, which is consistent with its enhanced photovoltaic performance in PSCs.

To probe the chemical composition throughout the film PDINB/PM6:Y6/PEDOT:PSS/ITO, the time of flight secondary ion mass spectrometry (TOF-SIMS) was performed by using the positive model under gas cluster ion beam (GCIB) method.[31] As shown in **Figure 5**a, the PDINB layer is first detected, and then the PM6:Y6 and PEDOT:PSS layers are demonstrated, respectively; while the ITO layer is not detected in the whole process. This TOF-SIMS analysis can verify that the PDINB layer is evenly deposited on the active layer, which would be beneficial for improving the photovoltaic performance in PSCs. Furthermore, through the 3D modulation as presented in Figure 5b,c, the interface between the PDINB layer and the active layer is quite distinct and clear in comparison with that between PEDOT:PSS and the active layer, which agrees well with the smooth surface of PDINB indicated by AFM images and is beneficial for the deposition of Ag.

2.4. Theoretical Calculation and Work Function Test

The work functions (WFs) of the cathode are determinative for the performance of PSCs. To understand the influence of PDINB on the electronic performance of Ag cathode, WFs were theoretically simulated and experimentally probed by an ultra-violet photoelectron spectrometer (UPS). As displayed in **Figure 6**a–d, the calculated WF of pristine Ag (111) is 4.46 eV, which agrees well with the published results.[32] Through introducing PDINB on the Ag interface, the calculated WF is decreased to 4.27, 0.19 eV lower than that of pristine Ag (111). This obvious reduction of WF via the modification of PDINB is ascribed to the existence of an amino group, where the N-group in amino could form an efficient interfacial dipole between the PDINB layer and the Ag electrode.[33] This interfacial dipole interaction is possibly ascribed to the interfacial chemisorption between PDINB layer and Ag. As a result, the electron density near the interface would be redistributed. Herein, a theoretical calculation of electron density distribution was carried out, as presented in Figure 6c. From the calculated data, it is shown that there is an apparent electron transfer process occurred from the PDINB layer to Ag, leading to a distinct electron density variation (a positive electrostatic peak at the Ag side and a negative electrostatic peak around the PDINB side) near the cathode interface (≈6 Å). This result indicates that the electron transfer process would occur in ≈ 6 Å length, which is the nature of interfacial dipole. Based on the calculation of

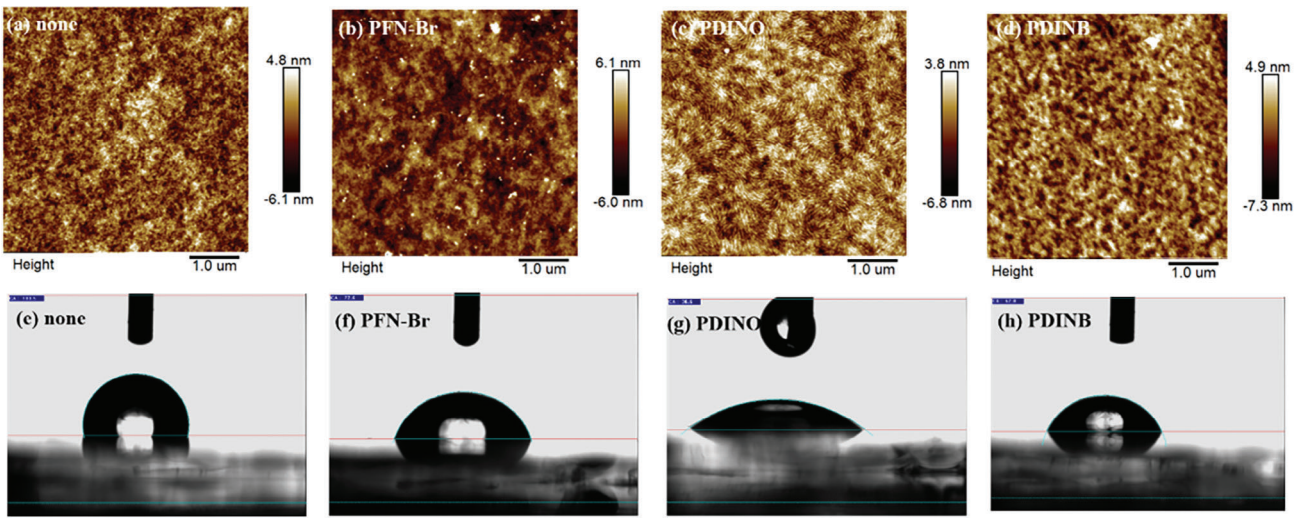

Figure 4. Surface topographic AFM images (size: 5 μm × 5 μm) of: a) pristine, b) PFN-Br, c) PDINO, and d) PDINB; and contact angle images: e) pristine, f) PFN-Br, g) PDINO, and h) PDINB modified active layers.

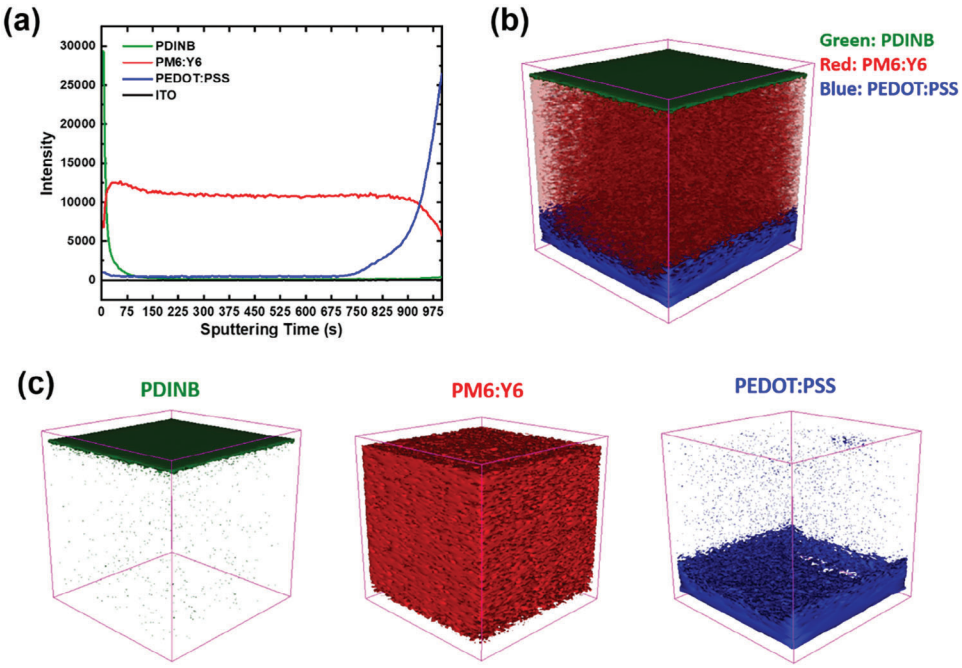

Figure 5. TOF-SIMS analysis: a) depth profile of the film of PDINB/PM6:Y6/PEDOT:PSS/ITO showing ion intensity as a function of sputtering time, b) the modulated 3D model of total three layers, and c) the modulated 3D models of every single layer including PDINB, PM6:Y6 and PEDOT:PSS, respectively.

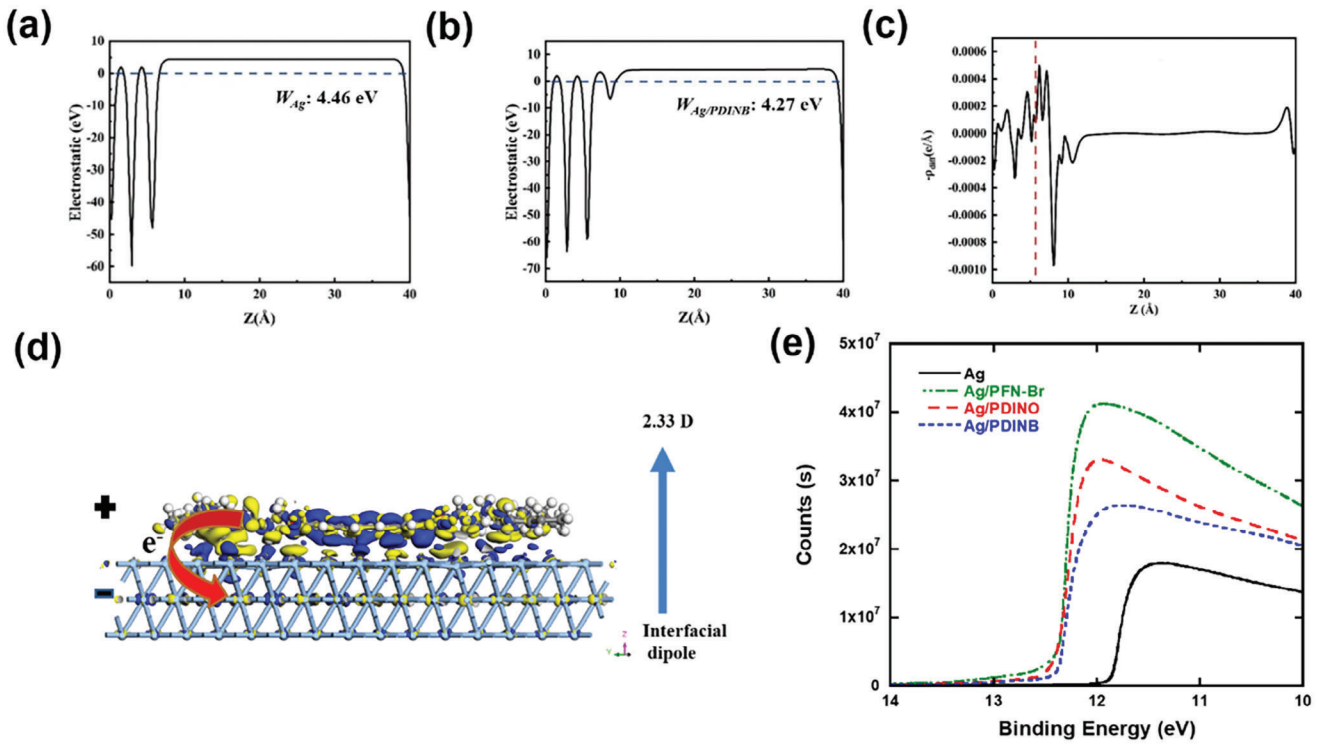

Figure 6. The work functions of theoretical calculation for a) neat Ag, b) PDINB modified Ag, c) charge density redistribution along the surface normal (z) averaged over the xy plane of PDINB on the surface of Ag (111), and d) proposed work mechanism of the interfacial dipoles of PDINB on the surface of Ag (111); e) the UPS curves of neat Ag and different ETLs modified Ag electrodes.

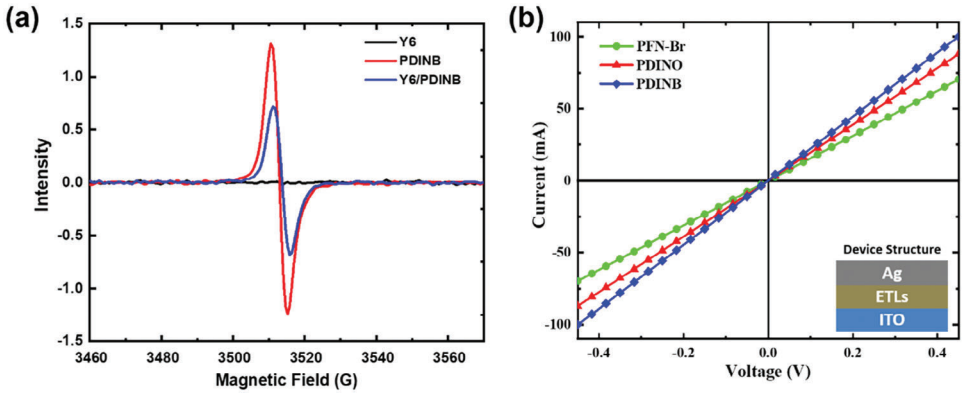

Figure 7. a) The EPR curves, and b) the conductivity curves of the devices with the structure of ITO/ETLs/Ag.

electron density distribution, it coincides with the above WFs calculation, implying that there exists a very strong electronic interaction at the interface. In order to further elucidate the intrinsic mechanism of forming interfacial dipole, the interface dipole Δμ is calculated, as shown in Figure 6d. Through the DFT calculation, the interface exhibits Δμ of 2.33 D with the upward direction from Ag to PDINB, which definitely decreases the WF of Ag cathode.[31] To demonstrate the theoretical results on decrement of WF, the UPS measurement was performed, as shown in Figure 6e. Compared with the WF of 4.34 eV of pristine Ag, the WFs are decreased to 3.83, 3.79, and 3.82 eV for PFN-Br, PDINO, and PDINB modified Ag electrode, respectively. Obviously, the interfacial modification of Ag by ETLs can effectively decrease the WFs, attributing to the existence of polar groups in the ETLs and the formation of right interfacial dipoles between ETLs and metal-based cathodes. Consequently, these reduced WFs would facilitate electron extraction and block hole transport, leading to higher FF and PCEs in the PSCs, which coincides with the obtained high photovoltaic performance.

2.5. Electron Paramagnetic Resonance and Conductivity Characterization

It has been reported that amino or halogen groups as side chains would achieve self-doped backbones, which would improve the electron-transport properties and molecular conductivities.[34,35] In this case, the electron paramagnetic resonance (EPR) measurement was carried out to evaluate the n-doping process of ETLs with Y6.[36] As the EPR spectra of pristine Y6, PDINB, and the mixture of Y6/PDINB with 1:1 weight ratio shown in **Figure 7a**, there is no detectable absorption signal for pure Y6, but the pure PDINB gives a very strong EPR signal at ≈ 3510 G, suggesting the efficient self-doping, namely, electron transfers from amino groups to the PDINB backbone. When PDINB is mixed with Y6, the EPR signal is weakened, however they still keep a strong signal response. Among the EPR test, it is noted that the doping mechanism of PDINB is mainly a self-doping process, not the doping from PDINB to the Y6 acceptor. Hence, the charge-transport loss at the PDINB layer might be reduced by this self-doping interaction, which would improve the FFs of PSCs.[32] To further understand the charge-transport properties, the ETLs-based device conductivities were characterized under the device architecture of ITO/ETLs/Ag, and the related conductivity curves were presented in Figure 7b.[37] It features that the PDINB-based device shows the highest conductivity than those of PFN-Br and PDINO, ascribing to the strong self-doping characteristic, matched energy alignment, and good film formability of PDINB. Therefore, this highest conductivity can, in part, elucidate the best photovoltaic performance of PDINB-based PSCs compared to the other two ETLs.

2.6. Charge Carrier Transport and Recombination Dynamics

It is widely noted that the introduction of efficient cathode interfacial layers (CILs) or electron-transport layers (ETLs) would enhance the photovoltaic performance dramatically in PSCs, resulting from their unique characteristics in good ohmic contact, effective charge carrier transport, and reduced charge carrier recombination. To study the charge recombination mechanism of the PSCs with different ETLs, the J_{sc}s and V_{oc}s of PSCs with PFN-Br, PDINO, and PDINB as ETLs under different light intensities were characterized, as presented in **Figure 8a,b**. The V_{oc}s-light intensity characteristics should follow the formula of $V_{OC} \propto nkT\ln(I)/q$, where k, T, I, and q are Boltzmann constant, Kelvin temperature, light intensity, and elementary charge, respectively. It is known that the slope of the lines could reflect the interfacial bimolecular recombination at open-circuit state. When the undesirable bimolecular recombination is occurred, namely Shockley-Read-Hall (SRH) recombination, the slope constant would be higher than kT/q. From Figure 8a, the four slopes are located at 1.20, 1.15, 1.18, and 1.01kT/q for the devices with the ETL of none, PFN-Br, PDINO, and PDINB, respectively. Clearly, the devices with the ETLs including PFN-Br, PDINO, and PDINB present lower slopes comparing to that without ETL. These results suggest that the introduction of functional ETLs could abate the trap-involved recombination, where the PDINB exhibits the better performance with lower recombination. Therefore, it manifests that PDINB can effectively inhibit interfacial trap-assisted recombination for PSCs. Additionally, in order to investigate the trap-assistant recombination in these devices, the relationship between J_{SC} and light intensity was also deduced, where it complied with the power law ($J_{SC} \propto I^{\alpha}$), where α is an exponential

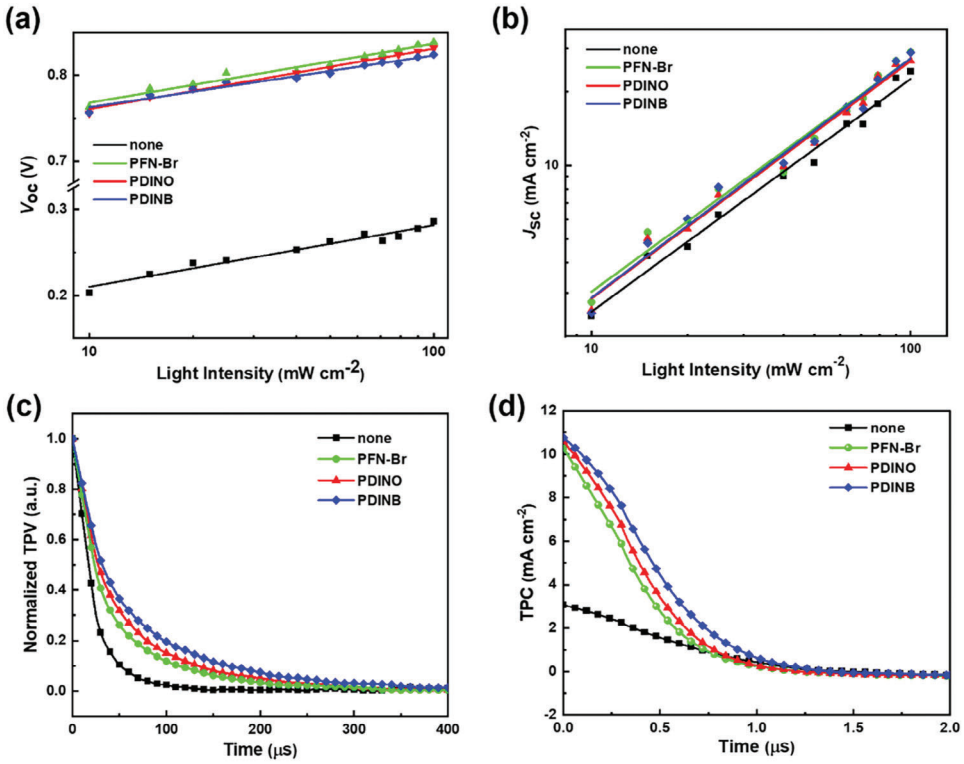

Figure 8. Charge carrier dynamics with different ETLs: a) V_{oc}-light intensity (ln I) and b) J_{sc}-light intensity characteristics; c) TPV-time and d) TPC-time characteristics.

factor. It is noted that when the value of α is close to 1, it suggests the bimolecular recombination is minimized. From Figure 8b, the fitted α values are recorded as 0.93, 0.95, 0.97, and 0.98 for the devices without ETL, and with PFN-Br, PDINO, and PDINB as ETLs, respectively. Compared with the device without ETL, the α values with ETLs modification are closer to 1, which means that the photo-generated charge carriers with ETLs could be efficiently extracted and collected by electrodes under the short-circuit state. In other words, the photo-generated charge carriers would be effectively swept out from active layer and interfaces prior to recombination. As mentioned above, the advantages of PDINB can also be reflected in the dark J–V curves and V_{eff}-J_{ph} curves, as shown in Figures S8 and S9 (Supporting Information), respectively. In Figure S8 (Supporting Information), it is noted that the PDINB-based device exhibited a lower dark current and advanced rectification ratio, which can be attributed to the better interfacial ohmic contact and lower interfacial recombination. As presented in Figure S9 (Supporting Information), the device with PDINB exhibits the best exciton dissociation rate of 99.1% compared to devices without ETL, with PFN-Br, and with PDINO of 94.9%, 98.6% and 98.1%, respectively. Among these results, it can be concluded that both of PFN-Br and PDINO can work as useful ETLs for non-fullerene PSCs, which are similar to the published device performance.[22,38] Interestingly, PDINB shows more effective suppression of bimolecular recombination in comparison to the other two ETLs, which implies that PDINB is a promising candidate for replacing the unstable and expensive ETLs available in the market.

To further explore the charge carrier extraction and recombination process, the transient photovoltage (TPV) and transient photocurrent (TPC) tests were further implemented, as shown in Figure 8c,d.[39,40] To carry out the measurement of TPV and TPC, all of these devices were tested under constant illumination of the solar simulator, when a small perturbation from a pulse laser was used to produce a small photocurrent. For TPV, it is utilized to analyze the related charge recombination lifetime. From Figure 8c, it shows that the devices with PFN-Br, PDINO, and PDINB as ETLs achieve a charge recombination decay lifetime of 10.95, 12.68, and 16.23 μs, respectively, which are much longer than that of 7.59 μs from the one without any ETLs. This implies that the introduction of ETLs can efficiently suppress the charge recombination. Furthermore, the PDINB shows the highest decay lifetime than the other two devices deposited with PFN-Br and PDINO, respectively, indicating that PDINB exhibits better capability in improving charge transport and inhibiting charge recombination for realizing high-performance PSCs. In addition, the TPC decay test was also performed to characterize the charge extraction dynamics in the related devices, and the typical TPC spectra were displayed in Figure 8d. Based on the TPC curves, the calculated amount of the extracted charge carriers from devices under laser excitation are 1.6×10^{-12}, 1.82×10^{-9}, 2.71×10^{-9} and 3.34×10^{-9} C for the devices without ETL, and with PFN-Br, PDINO, and PDINB as ETLs, respectively. Compared with the pristine device without any ETL, the devices with ETLs of PFN-Br, PDINO, and PDINB display higher amount of extracting charge carriers. Among them, PDINB gains the greatest extraction of charge carriers, implying that the fastest charge-extraction

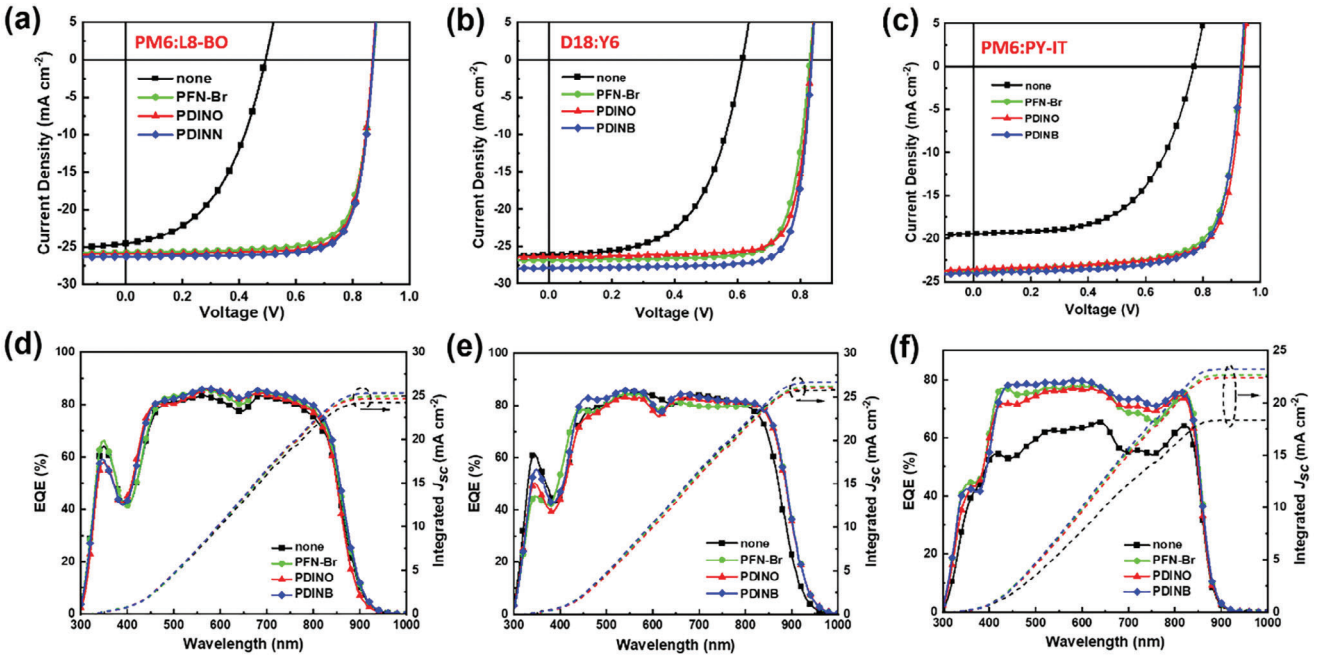

Figure 9. The device performances from different active layers with different ETLs: a–c) *J–V* curves of PSCs with none, PFN-Br, PDINO and PDINB as ETLs, respectively; d–f) EQE curves of PSCs with none, PFN-Br, PDINO and PDINB as ETLs, respectively.

process is achieved after depositing PDINB as ETL. This accelerated charge-extraction process is possibly originated from the better interfacial contact and matched energy alignment between active layer and cathode when PDINB is used as an ETL.[41] Overall, all the above investigations on TPV and TPC reveal that the outstanding photovoltaic performance from PDINB as ETL could be ascribed to its intrinsic ability to qualify the charge transport and inhibit charge recombination simultaneously.

2.7. Broad Applicability of PDINB as ETLs in PSCs

To explore the broad applicability of PDINB as an ETL for PSCs with different active materials, state-of-the-art active materials including PM6:L8-BO, D18:Y6, and a polymer:polymer (PM6:PY-IT) blend, were selected and their chemical structures were presented in Figure S10 (Supporting Information). For comparison, PSCs without ETL and with PFN-Br and PDINO as ETLs were also fabricated. The related *J–V* and EQE curves were shown in **Figure 9**, and the photovoltaic performance data were summarized in **Table 3**. Interestingly, all of these three systems with PDINB as an ETL give the highest photovoltaic performance among the PSCs with different ETLs, where the devices based on PM6:L8-BO, D18:Y6, and PM6:PY-IT present PCEs of 18.17%, 18.81%, and 16.72%, respectively. To verify the accuracy of the photovoltaic measurement, the PCE of the D18:Y6 system was certified as 18.39%, which is close to our result of 18.81% (Figure S11, Supporting Information).[42,43] These performances

Table 3. Summary of photovoltaic performances of PSCs based on different active layers with various ETLs under AM 1.5 G, 100 mW cm^{-2}.

Active Layers	ETLs	V_{oc} [V]	J_{sc} [mA cm^{-2}]	$J^{b)}_{sc}$ [mA cm^{-2}]	FF [%]	PCE $_{avg}$ $^{a)}$ [%]	PCE$_{max}$ [%]
PM6:L8-BO	none	0.49	24.64	24.26	46.98	5.49 (±0.23)	5.72
	PFN-Br	0.88	25.86	24.97	76.34	17.01 (±0.14)	17.30
	PDINO	0.87	25.89	24.71	78.39	17.59(±0.14)	17.75
	PDINB	0.88	26.43	25.34	78.44	18.08 (±0.11)	18.17
D18:Y6	none	0.62	25.97	25.75	56.15	8.62 (±0.45)	9.07
	PFN-Br	0.83	26.83	26.22	78.08	17.18 (±0.20)	17.40
	PDINO	0.83	26.43	26.03	79.28	17.26 (±0.17)	17.48
	PDINB	0.84	27.92	26.72	80.62	18.62 (±0.19)	18.81
PM6:PY-IT	none	0.77	19.43	18.37	58.14	8.51 (±0.41)	8.94
	PFN-Br	0.94	23.91	22.68	72.55	16.12 (±0.07)	16.22
	PDINO	0.94	23.55	22.43	74.99	16.41 (±0.11)	16.59
	PDINB	0.93	24.04	23.25	74.62	16.47 (±0.16)	16.72

$^{a)}$ the average PCE values from 10 individual devices; $^{b)}$ integrated J_{SC} from EQE curves.

are comparable to the PSCs reported for these material systems based on other ETLs.[14,44] These results indicate that PDINB can be a promising ETL material that may be widely used as ETL for PSCs with different active layer materials.

3. Conclusion

To conclude, a novel structured PDI derivative (PDINB) with amine-anchored long-side chains was designed and synthesized with very high yield (>97%) and low cost. PDINB shows high solubility in both nonpolar and polar organic solvents such as DCM and MeOH, due to the introduction of long side chains. Moreover, PDINB presents an interesting n-type self-doping effect and high conductivity as ETL. Ascribing to the existence of amine group, it can decrease the work function of the Ag cathode from 4.34 to 3.82 eV, which is beneficial for forming preferable ohmic contact between ETL and cathode. When PDINB is utilized as ETLs in PSCs, it presents very high photovoltaic performance with simultaneous enhancement in V_{oc}s, J_{sc}s, and FFs. Furthermore, the PSCs with PDINB as ETLs can retain 96% of their peak PCE when the ETL thickness varies from 5 to 30 nm. This insensitivity to the thickness of the ETL is particularly crucial for flexible large-scale roll-to-roll processing techniques. To further improve the thickness-tolerance ability of PDINB as an ETL in PSCs, chemical modifications can be implemented to enhance the conductivity and electron mobility, for instance, introducing stable radical molecules to the backbone.[25] Moreover, PDINB demonstrates broad applicability as ETLs for PSCs with diverse active layer materials, encompassing polymer: non-fullerene acceptors and all-polymer systems. Hence, the advantageous features of PDINB, including its low cost, thickness insensitivity, and broad applicability, position it as a highly promising ETL with the potential to advance the development of PSCs in the future.

4. Experimental Section

The details of material synthesis, characterization, device fabrication, and tests are presented in the supporting information.

Supporting Information

Supporting Information is available from the Wiley Online Library or from the author.

Acknowledgements

This work was supported by the National Natural Science Foundation of China (52373175), the High-level Innovative Talents Foundation of Guizhou Province (Grant No.QKHPTRC-GCC[2023]024), Science and Technology Innovation Team of Higher Education Department of Guizhou Province (Grant No.QJJ[2023]053), Natural Science Foundation of Guizhou University (GZUTGH[2023]12), Natural Science Foundation of Guizhou Province (CXTD[2023]005) and Wenner-Gren Foundations (UPD2021-0123). E. W. thanks the Swedish Research Council (2019-04683), the Swedish Research Council Formas (2020-01201), and The Knut and Alice Wallenberg Foundation (2022.0192) for financal support.

Conflict of Interest

The authors declare no conflict of interest.

Data Availability Statement

The data that support the findings of this study are available from the corresponding author upon reasonable request.

Keywords

electron transport layer, perylene diimide, polymer solar cells, self-doping, thickness-tolerant

Received: January 16, 2024
Revised: March 16, 2024
Published online:

[1] M. Wu, B. Ma, S. Li, J. Han, W. Zhao, *Adv. Funct. Mater.* **2023**, *33*, 2305445.
[2] L. Zhu, M. Zhang, J. Xu, C. Li, J. Yan, G. Zhou, W. Zhong, T. Hao, J. Song, X. Xue, Z. Zhou, R. Zeng, H. Zhu, C.-C. Chen, R. C. I. MacKenzie, Y. Zou, J. Nelson, Y. Zhang, Y. Sun, F. Liu, *Nat. Mater.* **2022**, *21*, 656.
[3] C. Guo, Y. Fu, D. Li, L. Wang, B. Zhou, C. Chen, J. Zhou, Y. Sun, Z. Gan, D. Liu, W. Li, T. Wang, *Adv. Mater.* **2023**, *35*, 2304921.
[4] R. Ma, M. Zeng, Y. Li, T. Liu, Z. Luo, Y. Xu, P. Li, N. Zheng, J. Li, Y. Li, R. Chen, J. Hou, F. Huang, H. Yan, *Adv. Energy Mater.* **2021**, *11*, 2100492.
[5] G. Li, V. Shrotriya, J. Huang, Y. Yao, T. Moriarty, K. Emery, Y. Yang, *Nat. Mater.* **2005**, *4*, 864.
[6] Y. Lin, Q. He, F. Zhao, L. Huo, J. Mai, X. Lu, C.-J. Su, T. Li, J. Wang, J. Zhu, Y. Sun, C. Wang, X. Zhan, *J. Am. Chem. Soc.* **2016**, *138*, 2973.
[7] J. Yuan, Y. Zhang, L. Zhou, G. Zhang, H.-L. Yip, T.-K. Lau, X. Lu, C. Zhu, H. Peng, P. A. Johnson, M. Leclerc, Y. Cao, J. Ulanski, Y. Li, Y. Zou, *Joule* **2019**, *3*, 1140.
[8] J. Huang, H. Tang, C. Yan, G. Li, *Cell Rep. Phys. Sci.* **2021**, *2*, 100292.
[9] M. Zhang, X. Guo, W. Ma, H. Ade, J. Hou, *Adv. Mater.* **2015**, *27*, 4655.
[10] Q. Liu, Y. Jiang, K. Jin, J. Qin, J. Xu, W. Li, J. Xiong, J. Liu, Z. Xiao, K. Sun, S. Yang, X. Zhang, L. Ding, *Sci. Bull.* **2020**, *65*, 272.
[11] C. Sun, F. Pan, H. Bin, J. Zhang, L. Xue, B. Qiu, Z. Wei, Z.-G. Zhang, Y. Li, *Nat. Commun.* **2018**, *9*, 743.
[12] Y. Lin, J. Wang, Z.-G. Zhang, H. Bai, Y. Li, D. Zhu, X. Zhan, *Adv. Mater.* **2015**, *27*, 1170.
[13] Z. Luo, T. Liu, R. Ma, Y. Xiao, L. Zhan, G. Zhang, H. Sun, F. Ni, G. Chai, J. Wang, C. Zhong, Y. Zou, X. Guo, X. Lu, H. Chen, H. Yan, C. Yang, *Adv. Mater.* **2020**, *32*, 2005942.
[14] R. Sorrentino, E. Kozma, S. Luzzati, R. Po, *Energy Environ. Sci.* **2021**, *14*, 180.
[15] X. Li, W. Zhang, K. Usman, J. Fang, *Adv. Energy Mater.* **2018**, *8*, 1702730.
[16] Z. Yin, J. Wei, Q. Zheng, *Adv. Sci.* **2016**, *3*, 1500362.
[17] X. Ouyang, R. Peng, L. Ai, X. Zhang, Z. Ge, *Nat. Photon.* **2015**, *9*, 520.
[18] Y. Zhou, C. Fuentes-Hernandez, J. Shim, J. Meyer, A. J. Giordano, H. Li, P. Winget, T. Papadopoulos, H. Cheun, J. Kim, M. Fenoll, A. Dindar, W. Haske, E. Najafabadi, T. M. Khan, H. Sojoudi, S. Barlow, S. Graham, J.-L. Brédas, S. R. Marder, A. Kahn, B. Kippelen, *Science* **2012**, *336*, 327.
[19] Z. He, C. Zhong, X. Huang, W.-Y. Wong, H. Wu, L. Chen, S. Su, Y. Cao, *Adv. Mater.* **2011**, *23*, 4636.
[20] T. Yang, M. Wang, C. Duan, X. Hu, L. Huang, J. Peng, F. Huang, X. Gong, *Energy Environ. Sci.* **2012**, *5*, 8208.
[21] Z.-G. Zhang, B. Qi, Z. Jin, D. Chi, Z. Qi, Y. Li, J. Wang, *Energy Environ. Sci.* **2014**, *7*, 1966.

[22] J. Yao, B. Qiu, Z.-G. Zhang, L. Xue, R. Wang, C. Zhang, S. Chen, Q. Zhou, C. Sun, C. Yang, M. Xiao, L. Meng, Y. Li, *Nat. Commun.* **2020**, *11*, 2726.
[23] J. Yao, S. Ding, R. Zhang, Y. Bai, Q. Zhou, L. Meng, E. Solano, J. A. Steele, M. B. J. Roeffaers, F. Gao, Z.-G. Zhang, Y. Li, *Adv. Mater.* **2022**, *34*, 2203690.
[24] Z. Wu, C. Sun, S. Dong, X.-F. Jiang, S. Wu, H. Wu, H.-L. Yip, F. Huang, Y. Cao, *J. Am. Chem. Soc.* **2016**, *138*, 2004.
[25] J. Fang, Z. Zhang, Z. Zhang, Y. Han, D. Xia, C. Zhao, Y. Zhang, L. Wang, C. Xiao, S. You, Y. Wu, W. Li, *J. Mater. Chem. A* **2023**, *11*, 6574.
[26] X. Xiong, X. Xue, M. Zhang, T. Hao, Z. Han, Y. Sun, Y. Zhang, F. Liu, S. Pei, L. Zhu, *ACS Energy Lett.* **2021**, *6*, 3582.
[27] R. Xu, K. Zhang, X. Liu, Y. Jin, X.-F. Jiang, Q.-H. Xu, F. Huang, Y. Cao, *ACS Appl. Mater. Interfaces* **2018**, *10*, 1939.
[28] J. Wachsmuth, A. Distler, C. Liu, T. Heumüller, Y. Liu, C. M. Aitchison, A. Hauser, M. Rossier, A. Robitaille, M.-A. Llobel, P.-O. Morin, A. Thepaut, C. Arrive, I. McCulloch, Y. Zhou, C. J. Brabec, H.-J. Egelhaaf, *Sol. RRL* **2023**, *7*, 2300602.
[29] L. Sang, X. Chen, J. Fang, P. Xu, W. Tian, K. Shui, Y. Han, H. Wang, R. Huang, Q. Zhang, Q. Luo, C.-Q. Ma, *Adv. Funct. Mater.* **2023**, *33*, 2304824.
[30] E. L. K. Spooner, E. J. Cassella, J. A. Smith, T. E. Catley, S. Burholt, D. G. Lidzey, *ACS Appl. Mater. Interfaces* **2023**, *15*, 39625.
[31] S. Surana, T. Conard, C. Fleischmann, J. G. Tait, J. P. Bastos, E. Voroshazi, R. Havelund, M. Turbiez, P. Louette, A. Felten, C. Poleunis, A. Delcorte, W. Vandervorst, *J. Phys. Chem. C* **2016**, *120*, 28074.
[32] C. Feng, X. Wang, Z. He, Y. Cao, *Sol. RRL* **2021**, *5*, 2000753.
[33] C. Feng, X. Wang, G. Chen, B. Zhang, Z. He, Y. Cao, *Langmuir* **2021**, *37*, 4347.
[34] W.-J. Sun, Y.-T. Wang, Y. Zhang, B. Sun, Z.-Q. Zhang, M.-J. Xiao, X.-Y. Li, Y. Huo, J. Xin, Q. Zhu, W. Ma, H.-L. Zhang, *Angew. Chem., Int. Ed.* **2022**, *61*, 2022083.
[35] L. Chen, Y. Tan, X. Liu, Y. Chen, *Nano Energy* **2016**, *27*, 492.
[36] X. Yin, X. Liu, Y. Peng, W. Zeng, C. Zhong, G. Xie, L. Wang, J. Fang, C. Yang, *Adv. Funct. Mater.* **2019**, *29*, 1806125.
[37] D. Zhou, W. You, F. Yang, R. Chen, H. Xu, Y. Tong, B. Hu, L. Hu, Y. Xie, L. Chen, *ACS Appl. Mater. Interfaces* **2021**, *13*, 50187.
[38] X. Wen, Y. Zhang, G. Xie, R. Rausch, N. Tang, N. Zheng, L. Liu, F. Würthner, Z. Xie, *Adv. Funct. Mater.* **2022**, *32*, 2111706.
[39] G. Shao, M. S. Glaz, F. Ma, H. Ju, D. S. Ginger, *ACS Nano* **2014**, *8*, 10799.
[40] G. Chen, S. Liu, J. Xu, R. He, Z. He, H. Wu, W. Yang, B. Zhang, Y. Cao, *ACS Appl. Mater. Interfaces* **2017**, *9*, 4778.
[41] L. Hu, F. Wu, C. Li, A. Hu, X. Hu, Y. Zhang, L. Chen, Y. Chen, *Macromolecules* **2015**, *48*, 5578.
[42] J. Wang, Y. Wang, P. Bi, Z. Chen, J. Qiao, J. Li, W. Wang, Z. Zheng, S. Zhang, X. Hao, J. Hou, *Adv. Mater.* **2023**, *35*, 2301583.
[43] J. Fu, P. W. K. Fong, H. Liu, C.-S. Huang, X. Lu, S. Lu, M. Abdelsamie, T. Kodalle, C. M. Sutter-Fella, Y. Yang, G. Li, *Nat. Commun.* **2023**, *14*, 1760.
[44] C. Li, J. Zhou, J. Song, J. Xu, H. Zhang, X. Zhang, J. Guo, L. Zhu, D. Wei, G. Han, J. Min, Y. Zhang, Z. Xie, Y. Yi, H. Yan, F. Gao, F. Liu, Y. Sun, *Nat. Energy* **2021**, *6*, 605.